Enhancing Skin Cancer Diagnosis using Cubic Pythagorean Fuzzy Hypersoft Set with Salp Swarm Algorithm

Afef Selmi[1,*], Imène Issaoui[2]

[1] Department of Information Technology, College of Computer, Qassim University, Buraydah, Saudi Arabia.
[2] Unit of Scientific Research, Applied College, Qassim University, Buraydah, Saudi Arabia
Emails: a.selmi@qu.edu.sa, I.ISSAOUI@qu.edu.sa

Abstract

Due to the rapid increase in population density, medical sciences now face a major challenge in the automated detection of diseases. Intelligent system assists health personnel in earlier disease diagnosis and provides reliable treatment to reduce the fatality rates. Skin cancer is one of the most severe and deadliest kinds of cancer. A health professional uses dermoscopic images to manually diagnose skin tumors. This technique can be time-consuming and labor-intensive and needs a considerable level of expertise. The automatic recognition method is essential for the earlier diagnosis of skin tumors. In recent times, N-soft Set model has become widespread, which is a generalization of fuzzy set where all the elements have a membership value in the complement (0 to 1) and in the set (0 or 1). This study presents a Skin Cancer Diagnosis using Cubic Pythagorean Fuzzy Hypersoft Set (SCD-CPFHSS) technique. The presented SCD-CPFHSS technique performs identification of skin cancer using the application of NSs and metaheuristic algorithms. In the SCD-CPFHSS technique, neural architectural search network (NASNet) model derives feature extractors from the dermoscopic image. In addition, the efficacy of the NASNet model can be boosted by the design of salp swarm algorithm (SSA). For skin cancer recognition, the SCD-CPFHSS technique applies CPFHSS model. The experimental outcome of the SCD-CPFHSS methodology was validated using medical dataset. The extensive results pointed out that the SCD-CPFHSS technique reaches better results on skin cancer diagnosis

Keywords: Artificial intelligence, Skin Cancer; Fuzzy Hypersoft Set; NASNet; Salp Swarm Algorithm; Dermoscopic Images

1. Introduction

Several problems in fields like social, medical, environmental, and economic, where the human factor is effectual, include uncertainty imprecision, or subjectivity [1]. Presently, most of the researchers have functioned on dissimilar mathematical methods to state and resolve this kind of issue [2]. At first, the mathematical method put evolved to rapid the uncertainty issues appropriately is the fuzzy set (FS) theory [3]. Actually, most of the other mathematical techniques like rough set theory, intuitionistic FS theory, and neutrosophic set theory were presented, however the soft set (SS) method presented is sturdy and sufficient, which mains every method projected so far in order to deal with uncertainty [4]. Skin cancer (SC) is the main general kind of cancer, which starts with the unrestrained reproduction of skin cells. It mainly occurs due to the ultraviolet emission from tanning beds or sunshine, and it mainly affects skin cells to increase and develop malignant cancer [5].

The automatic classification of SC by medical image enhances a dermatologist's medical practice [8]. Owing to the essential difficulties of dermatology area, researchers are required to focus on their development work and execution of artificial intelligence (AI)-based technology proposed for the recognition SC [9]. The use of AI is to mainly classify SC, which has got major attention at present. Researchers have attained important development, mainly in the recognition of illness patterns in medical images via the execution of AI [8]. In dermatology field, AI applications and tools are presently being advanced with the objective of defining the difficulty of numerous

DOI: https://doi.org/10.54216/IJNS.250113
Received: April 25, 2024 Revised: June 01, 2024 Accepted: July 01, 2024

illnesses [9]. The AI tools are a growth of a computer technique, which will acquire on its individual and perform some tasks that allied to dermatology, like differentiating among dissimilar kinds of SC lesions [10].

Furthermore, HC features are employed in order to remove features from many sizes, textures, shapes, and colors, which are employed in order to identify SC [11]. Textural attributes deliver data about the spatial spread of tone variants in an assumed area and the connection among neighbouring pixels [12]. Texture is considered a vital part since it is measured as both practical and perceptive [13]. The efficiency of the visual appearance and image content is based on how it utilizes color well. The color features of imagery were removed utilizing color histogram. Presently, many researchers effectively recover and identify features from dermoscopic images utilizing DL methods [14]. CNN utilizes its deep layer as a feature extractor. Utilizing the training data, the CNN features are well-trained, while specialist's expertise HC features to define a specific set of features [15]. The requirement to calculate sources and the availability of vast training sets were the main hurdles to utilizing CNN as an effectual feature extraction.

This study presents a Skin Cancer Diagnosis using Cubic Pythagorean Fuzzy Hypersoft Set (SCD-CPFHSS) technique. The presented SCD-CPFHSS technique performs identification of skin cancer using the application of NSs and metaheuristic algorithms. In the SCD-CPFHSS technique, neural architectural search network (NASNet) model derives feature extractors from the dermoscopic image. In addition, the efficacy of the NASNet model can be boosted by the design of salp swarm algorithm (SSA). For skin cancer recognition, the SCD-CPFHSS technique applies CPFHSS model. The experimental outcomes of the SCD-CPFHSS methodology can be validated using medical dataset.

2. Literature Works

In [16], a mechanical computer-aided strategy has been projected. The proposed method contains a sequence of steps. At first, the input imageries endure pre-processing to improve their quality and eliminate suitable features. Next, these pre-processed imageries are served into GRU network, a kind of DL method recognized for its aptitude to seizure successive data. To enhance the GRU network performance, an amended alternative of the Orca Predation Algorithm (OPA) technique has been used. Saeed et al. [17] use variations of CNN to efficiently analyze and categorize numerous skin lesion kinds utilizing the innovative benchmark datasets. The dataset experienced severe pre-processing, which included using innovative AI models such as Generative Adversarial Network (GAN) and Enhanced Super-Resolution GAN (ESRGAN) for the purpose of augmentation. In [18], a new structure based on DL is proposed in this work. The projected method is called as SCDNet which unites Vgg-16 with CNN for the identification of dissimilar kinds of SC. Furthermore, the accuracy of the developed technique is also equated with the 4 advanced pre-trained classifiers in the medicinal field called AlexNet, Resnet-50, VGG-19, and Inception-v3.

Zareen et al. [19] projected a DL-based CNN and Recurrent Neural Network (CNN-RNN) method by a ResNet50 structure that is employed as the feature extraction to improve SC classification. Leveraging synergistic time-based sequence learning and spatial feature extraction, the method proves strong performance. Utilizing pre-trained ResNet50 for spatial data extractor and LSTM for time-based dependences, the method gets a higher typical detection accuracy, exceeding preceding techniques. Venugopal et al. [20] projected a deep neural networks (DNNs) method with perfected training and enhanced learning on dermoscopic imageries for SC recognition. A knowledge base to train the DL methods was built by uniting dissimilar datasets of dermoscopic. Transfer learning (TL) is executed for quicker training of the projected method on an imperfect training dataset.

In [21], a Jaya Artificial Ecosystem-based Optimizer-LeNet (JAEO-LeNet) structure has been proposed. The bilateral filter (BF) has been deployed in order to refine the skin imagery of input that is permitted for skin lesion segmentation utilizing TransUNet. The expansion of segmented skin lesion imageries are achieved from the enlarged image, then numerous features were removed. In DL method, LeNet is used for SC recognition from the removed features. The JAEO technique has been projected for fine-tuning the weight of LeNet to improve the recognition performance efficiently. Prasad et al. [22] projected the automatic SC detection model, i.e. Aquila Driving Training-Based optimizer (ADTBO) with SqueezeNet. The segmentation of SC was finished by the Minkowski-based dual networks, which it include Deep Joint and PsiNet segmentation.

3. The Proposed Model

In this paper, we have developed a novel SCD-CPFHSS methodology. The presented SCD-CPFHSS technique performs identification of skin cancer using the application of NSs and metaheuristic algorithms. Fig. 1 depicts the entire procedure of SCD-CPFHSS technique.

DOI: https://doi.org/10.54216/IJNS.250113
Received: April 25, 2024 Revised: June 01, 2024 Accepted: July 01, 2024

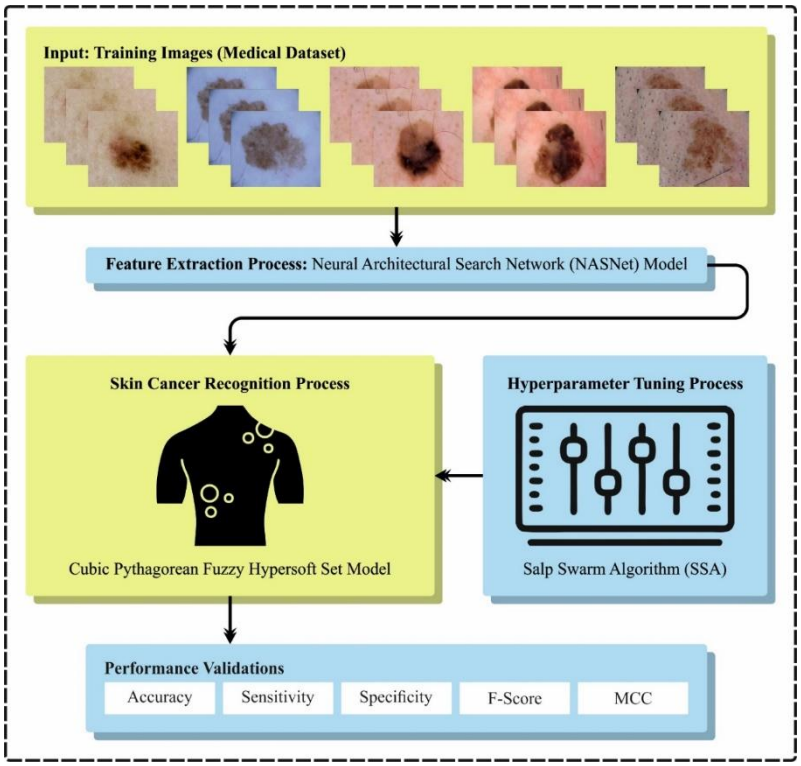

Figure 1: Overall process of SCD-CPFHSS technique

A. Feature Extraction

Initially, the SCD-CPFHSS technique undergoes the NASNet model to derive feature extractors from the dermoscopic image. Google Brain launches NASNet. Researchers of NASNet intended to find a building block on small data and move the blocks to the big data [23]. Mostly, the team first discovered an outstanding convolution layer on Canadian Institute for Advanced Research-10 data and later used it to ImageNet data by adding cells stacked on top of each other. Scheduled Drop Path, a regularization method is also proposed that improves the NASNet generalization. Lastly, the NASNet architecture achieves better outcomes with lower intricacy (FLOPs) and smaller model sizes. Fig. 2 depicts the structure of NASNet model.

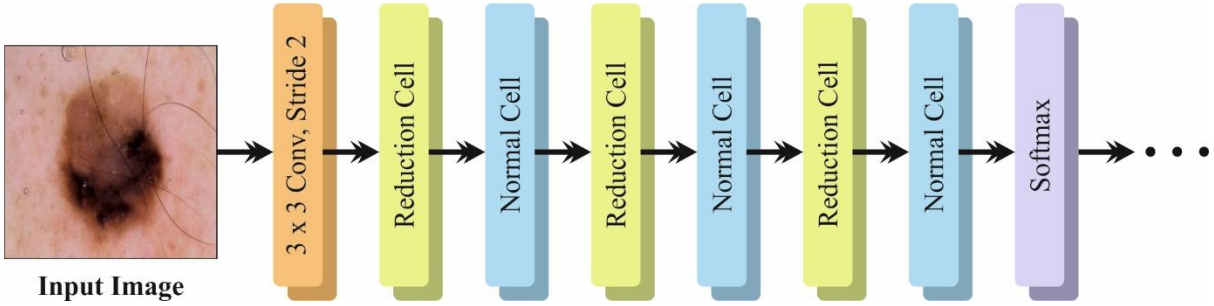

Figure 2: Architecture of NASNet

The pretrained NASNet model is used and assessed on hyperparameters including optimizer, batch size, and activation function that achieve the maximum accuracy amongst the present solution with less computation price.

- The best block is investigated by the model through reinforcement learning.
- N refers to the amount of motif repetitions which is free parameter together with convolution filter at initial step that is utilized for scaling.
- This cell is called reduction and normal cells. A normal cell is used to perform convolutional function and return the feature maps of similar size as input. The reduction cell is used to perform an operation related to max-pooling and return a mapping feature that is half the size of input in each dimension.
- The structure of normal and decrease cells is detected by the controller unit through the RNNs.

DOI: https://doi.org/10.54216/IJNS.250113
Received: April 25, 2024 Revised: June 01, 2024 Accepted: July 01, 2024

B. SSA-based Hyperparameter Tuning

Afterward, the efficacy of the NASNet model can be boosted by the design of SSA. SSA determines a mathematical expression of the salp chain [24]. Initially, the population was split into the leader and follower. The leader is the salp located at the front of chain, whereas the other are followers. The leader directs the swarm, whereas the follower adheres to one another, either indirectly or directly. Note that there is a food source F from the searching space that acts as the population's target.

The coefficient c_1 is an important features in SSA since it balances exploration and exploitation.

$$c_1 = 2e^{-\left(\frac{4l}{L}\right)^2} \tag{1}$$

Now l denotes the existing iteration, L shows the maximal iteration count. The parameters $c2$ and $c3$ are uniformly generated random numbers in [0,1]. This parameter plays a major role in defining whether the next location at j^{th} dimension must be directed to the negative or positive infinity, and influence the step size.

The following Eq. (2) is used for updating the position of leader x_j^1:

$$x_j^1 = \begin{cases} F_j + c_1\left((ub_j - lb_j)c + lb_j\right) c_3 \geq 0.5 \\ F_j - c_1\left((ub_j - lb_j)c + lb_j\right) c_3 < 05 \end{cases} \tag{2}$$

Here x_j^1 is the leader location at j^{th} dimension, F_j refers to the food source position at j^{th} dimension, ub_j and lb_j are the upper and lower boundaries of j^{th} dimensional, $c1, c2$, and c_3 are random numbers. The equation given in Eq. (2) keep to the boundary shown in the author's MATLAB code owing to conflicting literature based on the c_3 value within $c3 \geq 0.5$ vs. $c_3 \geq 0$,.

Eq. (3) is used for updating the follower location.

$$x_j^i = \frac{1}{2}\left(x_j^i + x_j^{i-1}\right) \tag{3}$$

If $i \geq 2$ and x_i^j refers to the location of i^{th} follower salps at j^{th} dimension.

The SSA enhances an FF to reach better classifier outcomes. It resolves a positive integer to suggest the good efficiency of candidate outcomes. In this case, the reduction of classifier error value has been assumes that FF.

$$fitness(x_i) = ClassifierErrorRate(x_i)$$
$$= \frac{No.\ of\ misclassified\ samples}{Total\ no.of\ samples} * 100 \tag{4}$$

C. Skin Cancer Recognition using CPFHSS model

For skin cancer recognition, the SCD-CPFHSS technique applies CPFHSS model. The concept of CPFHSS and certain factors of CC and WCC on CPFHSS are shown as follows [25].

A couple $\left(\Gamma, \widetilde{\Theta}\right)$ is known as a CPFHSS over $\mathcal{U}$, in case a mapping $\Gamma: \widetilde{\Theta} \to C^U$. CPFHSS is referred to as $\left(\Gamma, \widetilde{\Theta}\right) = \left\{\left(\tilde{\psi}, \Gamma\left(\tilde{\psi}\right)\right) \middle| \tilde{\psi} \in \widetilde{\Theta}, \Gamma\left(\tilde{\psi}\right) \in C^U\right\}$, where $\Gamma\left(\tilde{\psi}\right) = \left\{\left(\langle \tilde{\Upsilon}(u), \Upsilon_{\Gamma\left(\tilde{\psi}\right)}(u)\rangle, \langle \tilde{\Lambda}(u), \Lambda_{\Gamma\left(\tilde{\psi}\right)}(u)\rangle\right) | u \in \mathcal{U}\right\}$, where $\tilde{\Upsilon}(u): \mathcal{U} \to C[0,1], \tilde{\Lambda}(u): \mathcal{U} \to C[0,1]$, $\Upsilon_{\Gamma\left(\tilde{\psi}\right)}(u): \mathcal{U} \to [0,1]$ and $\Lambda_{\Gamma\left(\tilde{\psi}\right)}(u): \mathcal{U} \to [0,1]$. The lower and upper boundaries of $\tilde{\Upsilon}(u)$ and $\tilde{\Lambda}(u)$ are $\underline{\Upsilon}(u), \overline{\Upsilon}(u)$ and $\underline{\Lambda}_{\Gamma\left(\tilde{\psi}\right)}(u), \overline{\Lambda}(u)$, where $0 \leq (\overline{\Upsilon}(u))^2 + (\overline{\Lambda}(u))^2 \leq 1$ and $0 \leq (\Upsilon_{\Gamma\left(\tilde{\psi}\right)}(u))^2 + (\Lambda_{\Gamma\left(\tilde{\psi}\right)}(u))^2 \leq 1$.

Considering the current COVID19 outbreak, a psychiatrist's team assesses the student in two different terms in order to figure out the stress-coping level. The psychiatrist might have the following. (i) To authenticate the intuitionistic restriction condition for all the terms. (ii) To offers values in intervals for the initial term. (iii) To offer value in real numbers for the next term. Consider that the psychiatrists provide the value in interval for the

DOI: https://doi.org/10.54216/IJNS.250113
Received: April 25, 2024 Revised: June 01, 2024 Accepted: July 01, 2024

initial term, with $0 \leq (\overline{\Upsilon}(u))^2 + (\overline{\Lambda}(u))^2 \leq 1$ and in real value for the next term with $0 \leq (\Upsilon_{\Gamma(\tilde{\psi})}(u))^2 + (\Lambda_{\Gamma(\tilde{\psi})}(u))^2 \leq 1$. Integrate the value to form cubic Pythagorean fuzzy value.

Assume team of psychiatrists as $\mathcal{U} = \{\acute{p}_1, \acute{p}_2, \acute{p}_3, \acute{p}_4\}$. They are liable for examining students according to their academic stress-coping skills. Consider $\Theta_1, \Theta_2, \Theta_3$ and Θ_4 as attribute sets and sub-attributes as follows

Θ_1 =first stage= $\{\psi_{11}$ =sensitivity to stress,

Θ_2 =second stage= $\{\psi_{21}$ =capability for relaxation, ψ_{22} = self-reliance,

Θ_3 =third stage=$\{\psi_{31}$ =proactive mindset, ψ_{32} = versatility and adaptability } and

Θ_4 =last stage= $\{\psi_{41}$ =ability to assess situation.

Then $\tilde{\Theta} = \acute{\Theta}_1 \times \acute{\Theta}_2 \times \acute{\Theta}_3 \times \acute{\Theta}_4$ refers to the various attribute sets as follows

$$\tilde{\Theta} = \acute{\Theta}_1 \times \acute{\Theta}_2 \times \acute{\Theta}_3 \times \acute{\Theta}_4 = \{\acute{\psi}_{11}\} \times \{\acute{\psi}_{21}, \acute{\psi}_{22}\} \times \{\acute{\psi}_{31}, \acute{\psi}_{32}\} \times \{\acute{\psi}_{41}\}.$$

$$= \{\acute{\psi}_{11}, \acute{\psi}_{12}, \acute{\psi}i_{31}, \acute{\psi}_{41}), (\acute{\psi}_{11}, \acute{\psi}_{21}, \acute{\psi}_{32}, \acute{\psi}_{41}), (\acute{\psi}_{11}, \acute{\psi}_{22}, \acute{\psi}_{31}, \acute{\psi}_{41}), (\acute{\psi}_{11}, \acute{\psi}_{22}, \acute{\psi}_{32}, \acute{\psi}_{41})\}. = \left\{\tilde{\psi}_1, \tilde{\psi}_2, \tilde{\psi}_3, \tilde{\psi}_4\right\}.$$

Next, the value given by the psychiatrist for all the students is in the CPFHSS form.

Consider CPFHSS over $\mathcal{U}$ as follows.

$$(\Gamma_1, \tilde{\Theta}_1) = \{\left(u_i, \langle[\underline{\Upsilon}(u_i), \overline{\Upsilon}(u_i)], \Upsilon_{\Gamma_1(\tilde{\psi})}(u_i)\rangle, \langle[\underline{\Lambda}(u_i), \overline{\Lambda}(u_i)], \Lambda_{\Gamma_1(\tilde{\psi})}(u_i)\rangle\right\},$$

$$(\Gamma_2, \tilde{\Theta}) = \{\left(u_i, \langle[\underline{\Upsilon}(u_i), \overline{\Upsilon}(u_i)], \Upsilon_{\Gamma_2(\tilde{\psi})}(u_i)\rangle, \langle[\underline{\Lambda}(u_i), \overline{\Lambda}(u_i)], \Lambda_{\Gamma_2(\tilde{\psi})}(u_i)\rangle\right\}.$$

The CPFHSS energy of $(\Gamma_1, \tilde{\Theta})$ and $(\Gamma_2, \tilde{\Theta})$ are given below

$$\Phi(\Gamma_1, \tilde{\Theta}_1) = \sum_{k=1}^{u}\sum_{i=1}^{n}[\,(\underline{\Upsilon}_{\Gamma_1(\tilde{\psi}_k)}(u_i))^2 + (\underline{\Lambda}_{\Gamma_1(\tilde{\psi}_k)}(u_i))^2 + (\overline{\Upsilon}_{\Gamma_1(\tilde{\psi}_k)}(u_i))^2 + (\overline{\Lambda}_{\Gamma_1(\tilde{\psi}_k)}(u_i))^2$$
$$+(\Upsilon_{\Gamma_1(\tilde{\psi}_k)_{\Gamma_1(\tilde{\psi})}}(u_i))^2 + ((\Lambda_{\Gamma_1(\tilde{\psi})}(u_i))^2], \quad (5)$$

$$\Phi(\Gamma_2, \tilde{\Theta}_2) = \sum_{k=1}^{u}\sum_{i=1}^{n}[\,(\underline{\Upsilon}_{\Gamma_1(\tilde{\psi}_k)}(u_i))^2 + (\underline{\Lambda}(u_i))^2 + (\overline{\Upsilon}(u_i))^2 + (\overline{\Lambda}(u_i))^2$$
$$+(\Lambda_{\Gamma_2(\tilde{\psi})}(u_i))^2 + \left(\Lambda_{\Gamma_2(\tilde{\psi})}(u_i)\right)^2]. \quad (6)$$

The CC among $(\Gamma_1, \tilde{\Theta})$ and $(\Gamma_2, \tilde{\Theta})$ is shown below

$$C_\Upsilon((\Gamma_1, \tilde{\Theta}), (\Gamma_2, \tilde{\Theta})) = \sum_{k=1}^{u}\sum_{i=1}^{v}[\,(\underline{\Upsilon}_{\Gamma_1(\tilde{\psi}_k)}(u_i)) * (\underline{\Upsilon}_{\Gamma_2(\tilde{\psi}_k)}(u_i)) + (\Lambda_{\Gamma_1(\tilde{\psi})}(u_i)) * (\underline{\Lambda}_{\Gamma_2(\tilde{\psi}_k)}(u_i))$$
$$+\left(\overline{\Upsilon}_{\Gamma_1(\tilde{\psi}_k)}(u_i)\right) * \left(\overline{\Upsilon}_{\Gamma_2(\tilde{\psi}_k)}(u_i)\right) + \left(\overline{\Lambda}_{\Gamma_1(\tilde{\psi}_k)}(u_i)\right) * \left(\overline{\Lambda}_{\Gamma_2(\tilde{\psi}_k)}(u_i)\right) + \left(\Upsilon_{\Gamma_1(\tilde{\psi})}(u_i)\right)$$
$$* (\Upsilon_{\Gamma_2(\tilde{\psi})}(u_i)) + (\Lambda_{\Gamma_1(\tilde{\psi})}(u_i)) * (\Lambda_{\Gamma_2(\tilde{\psi})}(u_i))]. \quad (7)$$

Consider $(\Gamma_1, \tilde{\Theta}_1)$ and $(\Gamma_2, \tilde{\Theta}_2)$ as 2 CPFHSS. Next,

$$C_\Upsilon\left((\Gamma_1, \tilde{\Theta}_1), (\Gamma_1, \tilde{\Theta}_1)\right) = \Phi(\Gamma_1, \tilde{\Theta}_1)$$

$C_\Upsilon\left((\Gamma_2, \tilde{\Theta}_2), (\Gamma_2, \tilde{\Theta}_2)\right) = \Phi(\Gamma_2, \tilde{\Theta}_2)$.

The CC among $(\Gamma_1, \tilde{\Theta}_1)$ and $(\Gamma_2, \tilde{\Theta}_2)$ is

DOI: https://doi.org/10.54216/IJNS.250113
Received: April 25, 2024 Revised: June 01, 2024 Accepted: July 01, 2024

$$C_C((\Gamma_1,\tilde{\Theta}_1),(\Gamma_2,\tilde{\Theta}_2)) = \frac{C_Y\left((\Gamma_1,\tilde{\Theta}_1),(\Gamma_2,\tilde{\Theta}_2)\right)}{\sqrt{\Phi(\Gamma_1,\tilde{\Theta}_1)}\sqrt{\Phi(\Gamma_2,\tilde{\Theta}_2)}}$$

Assume $(\Gamma_1,\tilde{\Theta}_1)$ and $(\Gamma_2,\tilde{\Theta}_2)$ as CPFHSS. Next,

$0 \le C_C(\Gamma_1,\tilde{\Theta}_1),(\Gamma_2,\tilde{\Theta}_2)) \le 1$;

$$C_C((\Gamma_1,\tilde{\Theta}_1),(\Gamma_2,\tilde{\Theta}_2)) = C_C\left((\Gamma_2,\tilde{\Theta}_2),(\Gamma_1,\tilde{\Theta}_1)\right)$$

If $(\Gamma_1,\tilde{\Theta}_1) = (\Gamma_2,\tilde{\Theta}_2)$, then $C_C((\Gamma_1,\tilde{\Theta}_1),(\Gamma_2,\tilde{\Theta}_2)) = 1$.

Obliviously, $C_C((\Gamma_1,\tilde{\Theta}_1),(\Gamma_2,\tilde{\Theta}_2)) \ge 0$.

Hence, we prove $C_C((\Gamma_1,\tilde{\Theta}_1),(\Gamma_2,\tilde{\Theta}_2)) \le 1$.

$$C_T\left((\Gamma_1,\tilde{\Theta}_1),(\Gamma_2,\tilde{\Theta}_2)\right)$$

$= \sum_{p=1}^{u}\sum_{q=1}^{v}[\,(\underline{Y}_{\Gamma_1(\tilde{\psi}_p)}(u_q)) * (\underline{Y}_{\Gamma_2(\tilde{\psi}_p)}(u_q)) + (\underline{\Lambda}_{\Gamma_1(\tilde{\psi}_p)}(u_q)) * (\underline{\Lambda}_{\Gamma_2(\tilde{\psi}_p)}(u_q)) + (\overline{Y}_{\Gamma_1(\tilde{\psi}_p)}(u_q)) * (\overline{Y}_{\Gamma_2(\tilde{\psi}_p)}(u_q))$
$+(\overline{\Lambda}_{\Gamma_1(\tilde{\psi}_p)}(u_q)) * (\overline{\Lambda}_{\Gamma_2(\tilde{\psi}_p)}(u_q)) + (Y_{\Gamma_1(\overline{\psi})}(u_q)) * (Y_{\Gamma_2(\overline{\psi})}(u_q)) + (\Lambda_{\Gamma_1(\overline{\psi})}(u_q)) * (\Lambda_{\Gamma_2(\overline{\psi})}(u_q))]$.

$= \sum_{p=1}^{u}[\,((\underline{Y}_{\Gamma_1(\tilde{\psi}_p)}(u_1)) * (\underline{Y}_{\Gamma_2(\tilde{\psi}_p)}(u_1)) + (\Lambda_{\Gamma_1(\overline{\psi}_p)}(u_1)) * (\underline{\Lambda}_{\Gamma_2(\tilde{\psi}_p)}(u_1)) + (\overline{Y}_{\Gamma_1(\tilde{\psi}_p)}(u_1)) * (\overline{Y}_{\Gamma_2(\tilde{\psi}_p)}(u_1)) +$
$(\overline{\Lambda}_{\Gamma_1(\tilde{\psi}_p)}(u_1)) * (\overline{\Lambda}_{\Gamma_2(\tilde{\psi}_p)}(u_1)) + (Y_{\Gamma_1(\tilde{\psi}_p)}(u_1)) * (Y_{\Gamma_2(\tilde{\psi}_p)}(u_1)) + (\Lambda_{\Gamma_1(\tilde{\psi})}(u_1)) * (\Lambda_{\Gamma_2(\tilde{\psi}_p)}(u_1))) +$
$((\underline{Y}_{\Gamma_1(\tilde{\psi}_p)}(u_2)) * (\underline{Y}_{\Gamma_2(\tilde{\psi}_p)}(u_2)) + (\underline{\Lambda}_{\Gamma_1(\tilde{\psi}_p)}(u_2)) * (\Lambda_{\Gamma_2(\tilde{\psi}_p)}(u_2)) + (\overline{Y}_{\Gamma_1(\tilde{\psi}_p)}(u_2)) * (\overline{Y}_{\Gamma_2(\tilde{\psi}_p)}(u_2)) +$
$(\overline{\Lambda}_{\Gamma_1(\tilde{\psi}_p)}(u_2)) * (\overline{\Lambda}_{\Gamma_2(\tilde{\psi}_p)}(u_2)) + (Y_{\Gamma_1(\tilde{\psi}_p)}(u_2)) * (Y_{\Gamma_2(\tilde{\psi}_p)}(u_2)) + (\Lambda_{\Gamma_1(\tilde{\psi}_p)}(u_2)) * (\Lambda_{\Gamma_2(\tilde{\psi}_p)}(u_2))) +$
$+((\underline{Y}_{\Gamma_1(\tilde{\psi}_p)}(u_v)) * (\underline{Y}_{\Gamma_2(\tilde{\psi}_p)}(u_v)) + (\Lambda_{\Gamma_1(\tilde{\psi}_p)}(u_v)) * (\underline{\Lambda}_{\Gamma_2(\tilde{\psi}_p)}(u_v)) + (\overline{Y}_{\Gamma_1(\tilde{\psi}_p)}(u_v)) * (\overline{Y}_{\Gamma_2(\tilde{\psi}_p)}(u_v)) +$
$(\overline{\Lambda}(u_v)) * (\overline{\Lambda}_{\Gamma_2(\tilde{\psi}_p)}(u_v)) + (Y_{\Gamma_1(\tilde{\psi})}(u_v)) * (Y_{\Gamma_2(\tilde{\psi}_p)}(u_v)) + (\Lambda_{\Gamma_1(\tilde{\psi})}(u_v)) * (\Lambda_{\Gamma_2(\tilde{\psi}_p)}(u_v)))]$.

With Cauchy-Schwarz inequality, $C_M((\Gamma_1,\tilde{\Theta}_1),(\Gamma_2,\tilde{\Theta}_2))^2$

$$\le \sum_{p=1}^{u}[\,\{(\underline{Y}_{\Gamma_1(\tilde{\psi}_p)}(u_1))^2 + (\underline{Y}_{\Gamma_1(\tilde{\psi}_p)}(u_2))^2 + \cdots + \left(\underline{Y}_{\Gamma_1(\tilde{\psi}_p)}(u_v)\right)^2\}$$
$$+\{(\Lambda_{\Gamma_1(\tilde{\psi}_p)}(u_1))^2 + (\Lambda_{\Gamma_1(\tilde{\psi}_p)}(u_2))^2 + \cdots + \left(\Lambda_{\Gamma_1(\tilde{\psi}_p)}(u_v)\right)^2\}$$
$$+\{(\underline{Y}_{\Gamma_1(\tilde{\psi}_p)}(u_1))^2 + (\underline{Y}_{\Gamma_1(\tilde{\psi}_p)}(u_2))^2 + \cdots + \left(\underline{Y}_{\Gamma_1(\tilde{\psi}_p)}(u_v)\right)^2\}$$
$$+\{(\overline{\Lambda}_{\Gamma_1(\tilde{\psi}_p)}(u_1))^2 + (\overline{\Lambda}_{\Gamma_1(\tilde{\psi}_p)}(u_2))^2 + \cdots + (\overline{\Lambda}_{\Gamma_1(\tilde{\psi}_p)}(u_v))^2\}$$
$$+\{(\underline{Y}_{\Gamma_1(\tilde{\psi}_p)}(u_1))^2 + (\underline{Y}_{\Gamma_1(\tilde{\psi}_p)}(u_2))^2 + \cdots + (\underline{Y}_{\Gamma_1(\tilde{\psi}_p)}(u_v))^2\}$$
$$+\{(\overline{\Lambda}_{\Gamma_1(\tilde{\psi}_p)}(u_1))^2 + (\overline{\Lambda}_{\Gamma_1(\tilde{\psi}_p)}(u_2))^2 + \cdots + (\overline{\Lambda}_{\Gamma_1(\tilde{\psi}_p)}(u_v))^2\}$$
$$\times \sum_{p=1}^{u}[\,\{(\underline{Y}_{\Gamma_2(\tilde{\psi}_p)}(u_1))^2 + (\underline{Y}_{\Gamma_2(\tilde{\psi}_p)}(u_2))^2 + \cdots + (\underline{T}_{\Gamma_2(\tilde{\psi}_p)}(u_v))^2\}$$
$$+\{(\Lambda_{\Gamma_2(\tilde{\psi}_p)}(u_1))^2 + (\Lambda_{\Gamma_2(\tilde{\psi}_p)}(u_2))^2 + \cdots + (\Lambda_{\Gamma_2(\tilde{\psi}_p)}(u_v))^2\}$$
$$+\{(\underline{Y}_{\Gamma_2(\tilde{\psi}_p)}(u_1))^2 + (\underline{Y}_{\Gamma_2(\tilde{\psi}_p)}(u_2))^2 + \cdots + (\underline{T}_{\Gamma_2(\tilde{\psi}_p)}(u_v))^2\}$$
$$+\{(\Lambda_{\Gamma_2(\tilde{\psi}_p)}(u_1))^2 + (\Lambda_{\Gamma_2(\tilde{\psi}_p)}(u_2))^2 + \cdots + (\Lambda_{\Gamma_2(\tilde{\psi}_p)}(u_v))^2\}$$
$$+\{((\underline{Y}_{\Gamma_2(\tilde{\psi}_p)}(u_1))^2 + (\underline{Y}_{\Gamma_2(\tilde{\psi}_p)}(u_2))^2 + \cdots + (\underline{T}_{\Gamma_2(\tilde{\psi}_p)}(u_v))^2\}$$

DOI: https://doi.org/10.54216/IJNS.250113
Received: April 25, 2024 Revised: June 01, 2024 Accepted: July 01, 2024

$$+\{(\Lambda_{\Gamma_2(\tilde{\psi}_p)}(u_1))^2+(\Lambda_{\Gamma_2(\tilde{\psi}_p)}(u_2))^2+\cdots+(\Lambda_{\Gamma_2(\tilde{\psi}_p)}(u_v))^2\}].$$

$$C_M((\Gamma_1,\tilde{\Theta}_1),(\Gamma_2,\tilde{\Theta}_2))^2$$

$$\leq \sum_{p=1}^{u}\sum_{q=1}^{v}[\,(\underline{\Upsilon}_{\Gamma_1(\tilde{\psi}_p)}(u_q))^2+(\underline{\Lambda}_{\Gamma_1(\tilde{\psi}_p)}(u_q))^2+(\overline{\Upsilon}_{\Gamma_1(\tilde{\psi}_p)}(u_q))^2+(\overline{\Lambda}_{\Gamma_1(\tilde{\psi}_p)}(u_q))^2$$

$$+(\Upsilon_{\Gamma_1(\tilde{\psi}_p)}(u_q))^2+(\Lambda_{\Gamma_1(\tilde{\psi}_p)}(u_q))^2]\times\sum_{p=1}^{u}\sum_{q=1}^{v}[\,(\underline{\Upsilon}_{\Gamma_2(\tilde{\psi}_p)}(u_q))^2+(\Lambda_{\Gamma_2(\tilde{\psi}_p)}(u_q))^2$$

$$+(\overline{\Upsilon}_{\Gamma_2(\tilde{\psi}_p)}(u_q))^2+(\overline{\Lambda}_{\Gamma_2(\tilde{\psi}_p)}(u_q))^2+(T_{\Gamma_2(\tilde{\psi})}(u_q))^2+(\Lambda_{\Gamma_2(\tilde{\psi})}(u_q))^2].$$

$\Rightarrow C_M((\Gamma_1,\tilde{\Theta}),(\Gamma_2,\tilde{\Theta}_2))^2 \leq \Phi(\Gamma_1,\tilde{\Theta})\times\Phi(\Gamma_2,\tilde{\Theta}_2).$

$$\Rightarrow C_M((\Gamma_1,\tilde{\Theta}_1),(\Gamma_2,\tilde{\Theta}_2)) \leq \sqrt{\Phi(\Gamma_1,\tilde{\Theta}_1)}\times\sqrt{\Phi(\Gamma_2,\tilde{\Theta}_2)}.$$

$$\Rightarrow \frac{C_M((\Gamma_1,\tilde{\Theta}_1),(\Gamma_2,\tilde{\Theta}_2))}{\sqrt{\Phi(\Gamma_1,\tilde{\Theta}_1)}\times\sqrt{\Phi(\Gamma_2,\tilde{\Theta}_2)}}\leq 1.$$

Using $C_C((\Gamma_1,\tilde{\Theta}_1),(\Gamma_2,\tilde{\Theta}_2))\leq 1.$

Hence, $0\leq C_C((\Gamma_1,\tilde{\Theta}_1),(\Gamma_2,\tilde{\Theta}_2))\leq 1.$

Proof. (ii) Straightforward.

Proof. (iii) $C_C((\Gamma_1,\tilde{\Theta}_1),(\Gamma_2,\tilde{\Theta}_2))=\frac{C_M((\Gamma_1,\tilde{\Theta}_1),(\Gamma_2,\tilde{\Theta}_2))}{\sqrt{\Phi(\Gamma_1,\tilde{\Theta}_1)}\times\sqrt{\Phi(\Gamma_2,\tilde{\Theta}_2)}}.$

As, $(\Gamma_1,\tilde{\Theta}_1)=(\Gamma_2,\tilde{\Theta}_2).$

$$C_C((\Gamma_1,\tilde{\Theta}_1),(\Gamma_2,\tilde{\Theta}_2))$$

$$=\sqrt{\left\{\begin{array}{c}\sum_{p=1}^{u}\sum_{q=1}^{v}[\,(\underline{\Upsilon}_{\Gamma_2(\tilde{\psi}_p)}(u_q))^2+(\Lambda_{\Gamma_2(\tilde{\psi}_p)}(u_q))^2+(\overline{\Upsilon}_{\Gamma_2(\tilde{\psi}_p)}(u_q))^2\\ +(\overline{\Lambda}_{\Gamma_2(\tilde{\psi}_p)}(u_q))^2+(\Upsilon_{\Gamma_2(\tilde{\psi}_p)}(u_q))^2+\left(\Lambda_{\Gamma_2(\tilde{\psi}_p)}(u_q)\right)^2\right]\end{array}\right\}}$$

$$\times\sqrt{\left\{\begin{array}{c}\sum_{p=1}^{u}\sum_{q=1}^{v}[\,(\underline{\Upsilon}_{\Gamma_2(\tilde{\psi}_p)}(u_q))^2+(\underline{\Lambda}_{\Gamma_2(\tilde{\psi}_p)}(u_q))^2+(\overline{\Upsilon}_{\Gamma_2(\tilde{\psi}_p)}(u_q))^2+(\overline{\Lambda}_{\Gamma_2(\tilde{\psi}_p)}(u_q))^2+(\Upsilon_{\Gamma_2(\tilde{\psi}_p)}(u_q))^2\\ +\left(\Lambda_{\Gamma_2(\tilde{\psi}_p)}(u_q)\right)^2\right]\end{array}\right\}}$$

$\Rightarrow C_C((\Gamma_1,\tilde{\Theta}_1),(\Gamma_2,\tilde{\Theta}_2))=1.$

The CC among $(\Gamma_1,\tilde{\Theta}_1)$ and $(\Gamma_2,\tilde{\Theta}_2)$ is

$$\tilde{C}_C\left((\Gamma_1,\tilde{\Theta}_1),(\Gamma_2,\tilde{\Theta}_2)\right)=\frac{C_T((\Gamma_1,\tilde{\Theta}_1),(\Gamma_2,\tilde{\Theta}_2))}{\max\{\Phi(\Gamma_1,\tilde{\Theta}_1),\Phi(\Gamma_2,\tilde{\Theta}_2)\}}. \quad (8)$$

DOI: https://doi.org/10.54216/IJNS.250113
Received: April 25, 2024 Revised: June 01, 2024 Accepted: July 01, 2024

$$= \frac{\begin{array}{c}\sum_{p=1}^{u}\sum_{q=1}^{v}[\left(\underline{\Upsilon}_{\Gamma_1(\tilde{\psi}_p)}(u_q)\right)*\left(\underline{\Upsilon}_{\Gamma_2(\tilde{\psi}_p)}(u_q)\right)+\left(\underline{\Lambda}_{\Gamma_1(\tilde{\psi}_p)}(u_q)\right)*\left(\Lambda_{\Gamma_2(\tilde{\psi}_p)}(u_q)\right)\\ +\left(\overline{\Upsilon}_{\Gamma_1(\tilde{\psi}_p)}(u_q)\right)*\left(\overline{\Upsilon}_{\Gamma_2(\tilde{\psi}_p)}(u_q)\right)+\left(\overline{\Lambda}_{\Gamma_1(\tilde{\psi}_p)}(u_q)\right)*\left(\overline{\Lambda}_{\Gamma_2(\tilde{\psi}_p)}(u_q)\right)+\left(\Upsilon_{\Gamma_1(\tilde{\psi}_p)}(u_q)\right)*\left(\Upsilon_{\Gamma_2(\tilde{\psi}_p)}(u_q)\right)\\ +(\Lambda_{\Gamma_1(\tilde{\psi}_p)}(u_q))*(\Lambda_{\Gamma_2(\tilde{\psi}_p)}(u_q))]\end{array}}{\max\left\{\begin{array}{c}\sum_{p=1}^{u}\sum_{q=1}^{v}[(\underline{T}_{\Gamma_1(\tilde{\psi}_p)}(u_q))^2+(\underline{\Lambda}_{\Gamma_1(\tilde{\psi}_p)}(u_q))^2+(\overline{T}(u_q))^2+(\overline{\Lambda}_{\Gamma_1(\tilde{\psi}_p)}(u_q))^2+(\Upsilon_{\Gamma_1(\tilde{\psi}_p)}(u_q))^2\\ +\left(\Lambda_{\Gamma_1(\tilde{\psi}_p)}(u_q)\right)^2],\sum_{p=1}^{u}\sum_{q=1}^{v}[(\underline{\Upsilon}_{\Gamma_2(\tilde{\psi}_p)}(u_q))^2+(\Lambda_{\Gamma_2(\tilde{\psi}_p)}(u_q))^2+\left(\overline{\Upsilon}_{\Gamma_2(\tilde{\psi}_p)}(u_q)\right)^2\\ +(\overline{\Lambda}_{\Gamma_2(\tilde{\psi}_p)}(u_q))^2+(\Upsilon_{\Gamma_2(\tilde{\psi}_p)}(u_q))^2+(\Lambda_{\Gamma_2(\tilde{\psi}_p))}(u_q))^2]\end{array}\right\}},$$

4. Result Analysis

The experimental outcome of the SCD-CPFHSS methodology can be validated using ISIC2017 dataset. The dataset encompasses 2000 samples under 3 class labels are represented in Table 1.

Table 1: Details of database

ISIC 2017 Database		
Classes	Labels	No. of Instances
Melanoma	Class1	374
Seborrheic Keratosis	Class2	254
Nevus	Class3	1372
Total No. of Instances		2000

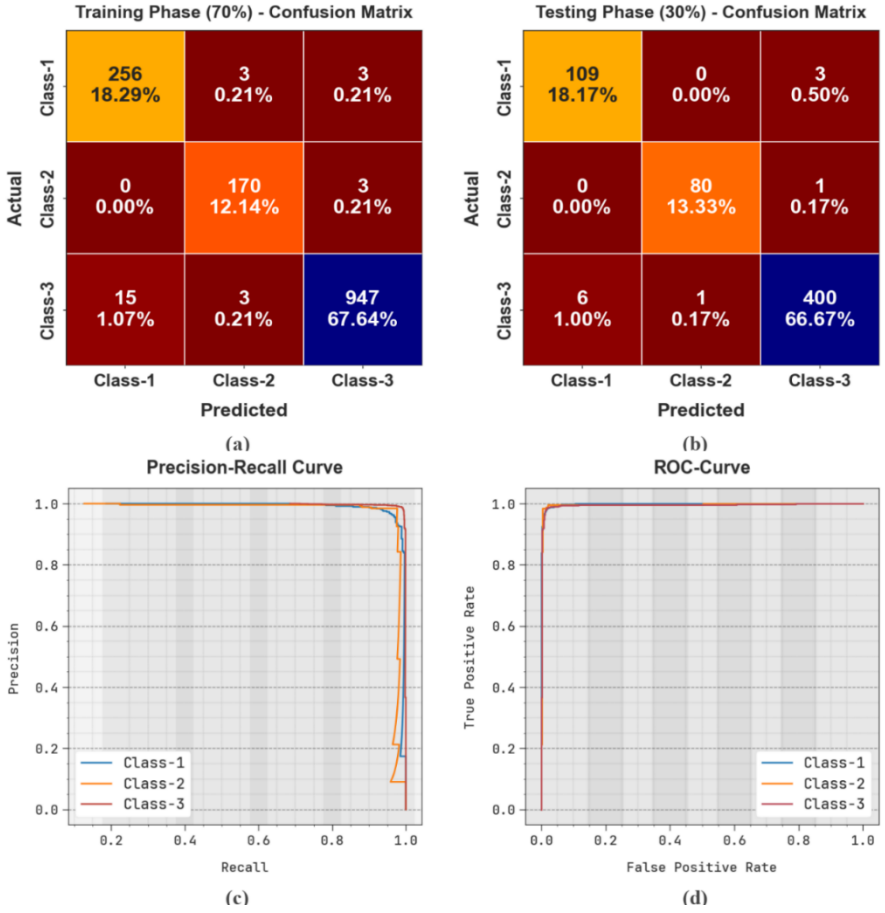

Figure 3: Classifier outcome of (a-b) Confusion matrices and (c-d) PR and ROC curves

DOI: https://doi.org/10.54216/IJNS.250113
Received: April 25, 2024 Revised: June 01, 2024 Accepted: July 01, 2024

Fig. 3 represents the classifier analysis of the SCD-CPFHSS model. Figs. 3a-3b describes the confusion matrices achieved by the SCD-CPFHSS method on 70%TRAS:30%TESS. The outcome defined that the SCD-CPFHSS approach has properly identified 3 classes. Next, Fig. 3c illustrates the PR outcome of the SCD-CPFHSS algorithm. The experimental values exhibited that the SCD-CPFHSS system has accomplished superior rate of PR at 3 classes. Nevertheless, Fig. 3d shows the ROC analysis of the SCD-CPFHSS model. The simulation outcome defined that the SCD-CPFHSS technique has directed to accomplished solutions with the enhanced value of ROC at 3 classes.

In Table 2 and Fig. 4, the skin cancer recognition outcome of the SCD-CPFHSS model is clearly depicted under 70%TRAS and 30%TESS. The results signified that the SCD-CPFHSS technique properly identified the three class samples. With 70%TRAS, the SCD-CPFHSS system reaches an average $accu_y$ of 98.71%, $sens_y$ of 98.04%, $spec_y$ of 98.94%, F_{score} of 97.41%, and MCC of 96.09%. In addition, with 30%TESS, the SCD-CPFHSS system reaches average $accu_y$ of 98.78%, $sens_y$ of 98.12%, $spec_y$ of 98.84%, F_{score} of 97.81%, and MCC of 96.51%.

Table 2: Skin cancer recognition outcome of SCD-CPFHSS technique under 70%TRAS and 30%TESS

Class Labels	$Accu_y$	$Sens_y$	$Spec_y$	F_{Score}	MCC
TRAS (70%)					
Class-1	98.50	97.71	98.68	96.06	95.15
Class-2	99.36	98.27	99.51	97.42	97.06
Class-3	98.29	98.13	98.62	98.75	96.05
Average	98.71	98.04	98.94	97.41	96.09
TESS (30%)					
Class-1	98.50	97.32	98.77	96.04	95.12
Class-2	99.67	98.77	99.81	98.77	98.57
Class-3	98.17	98.28	97.93	98.64	95.82
Average	98.78	98.12	98.84	97.81	96.51

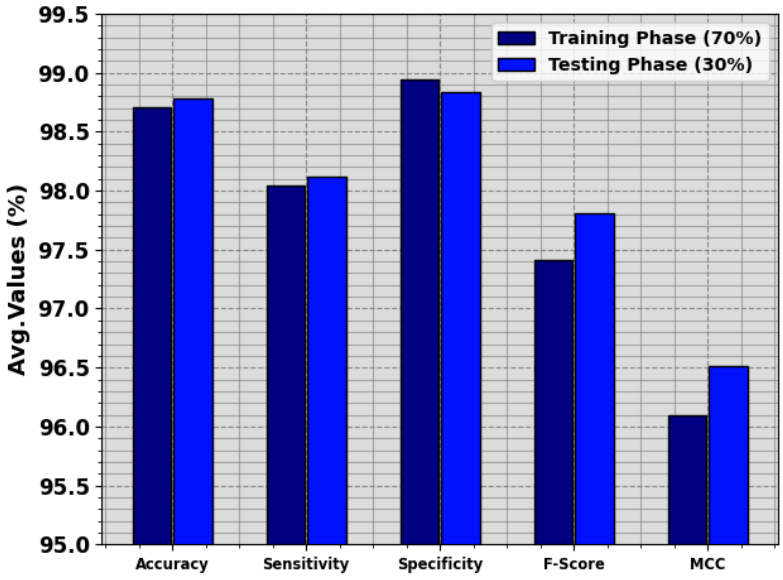

Figure 4: Average outcome of SCD-CPFHSS technique under 70%TRAS and 30%TESS

Table 3 demonstrates the comparison examination of the SCD-CPFHSS algorithm with existing models [26, 27]. Fig. 5 illustrates the $accu_y$ and F_{score} study of the SCD-CPFHSS methodology. The experimental outcome implies that the SCD-CPFHSS model has exhibited maximum performance. Based on $accu_y$, the SCD-CPFHSS technique has higher $accu_y$ of 98.78% while the AMCSCC-WHOEL, MAFCNN-SCD, NB, KELM, MSVM, MobileNet, and DenseNet169 approaches have lesser $accu_y$ of 98.36%, 92.27%, 89.81%, 88.07%, 87.18%, 85.07%, and 89.46%, respectively. In addition, based on F_{score}, the SCD-CPFHSS technique has superior F_{score} of 97.81% while the AMCSCC-WHOEL, MAFCNN-SCD, NB, KELM, MSVM, MobileNet, and DenseNet169 methodologies have minimal F_{score} of 96.08%, 83.08%, 81.40%, 83.23%, 81.47%, 81.23%, and 83.32%, correspondingly.

DOI: https://doi.org/10.54216/IJNS.250113
Received: April 25, 2024 Revised: June 01, 2024 Accepted: July 01, 2024

Table 3: Comparative outcome of SCD-CPFHSS model with existing systems

ISIC 2017 Dataset				
Methods	$Accu_y$	$Sens_y$	$Spec_y$	F_{Score}
SCD-CPFHSS	98.78	98.12	98.84	97.81
AMCSCC-WHOEL	98.36	95.61	98.23	96.08
MAFCNN-SCD	92.27	77.11	88.70	83.08
NB Classifier	89.81	74.74	84.06	81.40
KELM Algorithm	88.07	77.08	84.51	83.23
MSVM Method	87.18	75.47	83.21	81.47
MobileNet Model	85.07	74.19	88.01	81.23
DenseNet169	89.46	76.85	86.32	83.32

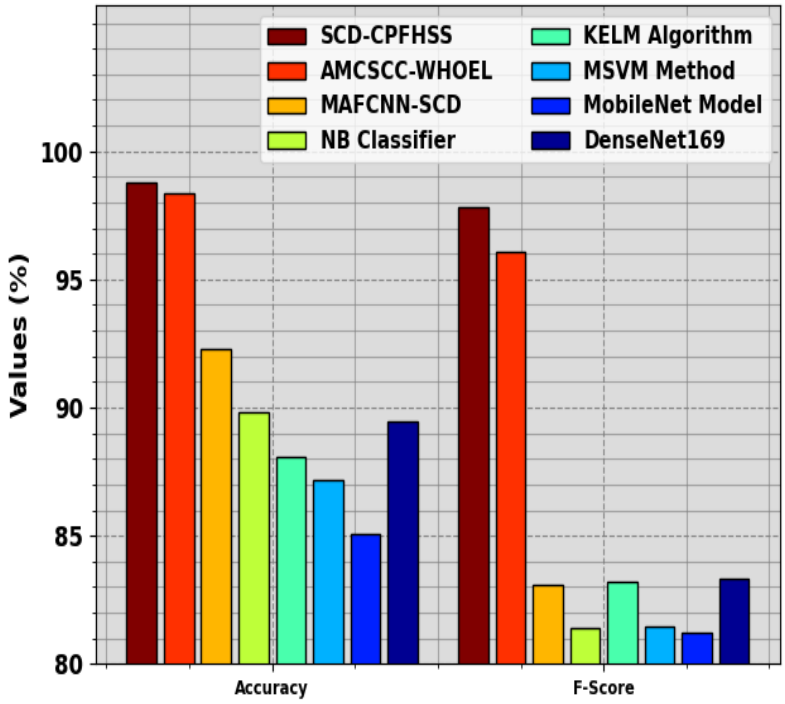

Figure 5: $Accu_y$ and F_{score} analysis of SCD-CPFHSS model with existing systems

Fig. 6 exemplifies the $sens_y$ and $spec_y$ analysis of the SCD-CPFHSS algorithm. The experimental outcome inferred that the SCD-CPFHSS model has demonstrated enhanced performances. Based on $sens_y$, the SCD-CPFHSS algorithm has higher $sens_y$ of 98.12% while the AMCSCC-WHOEL, MAFCNN-SCD, NB, KELM, MSVM, MobileNet, and DenseNet169 approaches have decreased $sens_y$ of 95.61%, 77.11%, 74.74%, 77.08%, 75.47%, 74.19%, and 76.85%, correspondingly. Additionally, based on $spec_y$, the SCD-CPFHSS algorithm has maximal $spec_y$ of 98.84% while the AMCSCC-WHOEL, MAFCNN-SCD, NB, KELM, MSVM, MobileNet, and DenseNet169 systems have minimal $spec_y$ of 98.23%, 88.70%, 84.06%, 84.51%, 83.21%, 88.01%, and 86.32%, correspondingly.

DOI: https://doi.org/10.54216/IJNS.250113
Received: April 25, 2024 Revised: June 01, 2024 Accepted: July 01, 2024

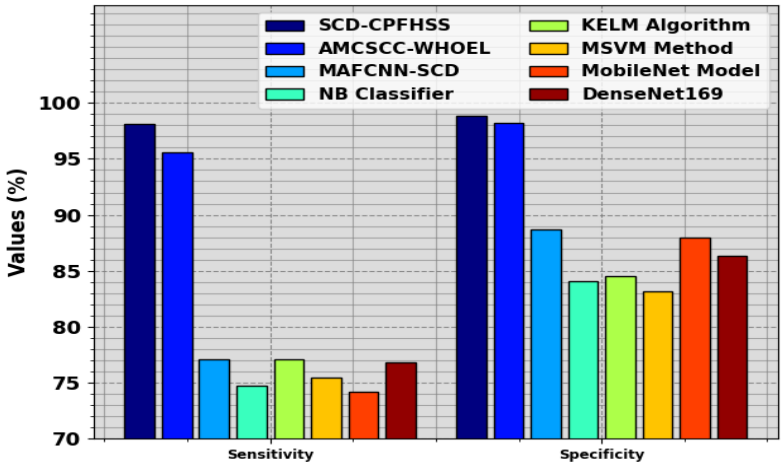

Figure 6: $Sens_y$ and $spec_y$ analysis of SCD-CPFHSS model with existing systems

The results ensured that the SCD-CPFHSS technique reaches better results on skin cancer diagnosis.

5. Conclusion

In this manuscript, we have developed a novel SCD-CPFHSS technique. The presented SCD-CPFHSS technique performs the identification of skin cancer using the application of NSs and metaheuristic algorithms. It contains three different kinds of processes involved. Initially, the SCD-CPFHSS technique undergoes the NASNet model to derive feature extractors from the dermoscopic image. In addition, the efficacy of the NASNet model can be boosted by the design of SSA. For skin cancer recognition, the SCD-CPFHSS technique applies the CPFHSS model. The experimental outcome of the SCD-CPFHSS methodology can be validated using a medical dataset. The extensive results pointed out that the SCD-CPFHSS technique reaches better results on skin cancer diagnosis.

Funding: "This research received no external funding"

Conflicts of Interest: "The authors declare no conflict of interest."

References

[1] Tuqa A. H. Al-Tamimi, Luay A. A. Al-Swidi , Ali H. M. Al-Obaidi. "Partner Sets for Generalizations of MultiNeutrosophic Sets." International Journal of Neutrosophic Science, Vol. 24, No. 1, 2024 ,PP. 08-13

[2] Noaman, I.A.R., Hasan, A.H. and Ahmed, S.M., 2024. Optimizing Weibull Distribution Parameters for Improved Earthquake Modeling in Japan: A Comparative Approach. International Journal of Neutrosophic Science, 24(1), pp.65-5.

[3] Doaa Nihad Tomma, L. A. A. Al-Swidi. "Necessary and Sufficient Conditions for a Stability of the Concepts of Stable Interior and Stable Exterior via Neutrosophic Crisp Sets." International Journal of Neutrosophic Science, Vol. 24, No. 1, 2024 ,PP. 87-93

[4] Mathews, P., Sebastian, L. and Thankachan, B., 2024. Neutrosophic Fuzzy Score Matrices: A Robust Framework for Advancing Medical Diagnostics. International Journal of Neutrosophic Science, 23(3), pp.08-8.

[5] R. Saarumathi, W. Ritha. (2024). A Legitimate Productive Repertoire Replica Betwixt Envirotech Outlay Towards Fragile Commodities Using Trapezoidal Neutrosophic Fuzzy Number. International Journal of Neutrosophic Science, 24 (1), 104-118

[6] Tahir, M., Naeem, A., Malik, H., Tanveer, J., Naqvi, R.A. and Lee, S.W., 2023. DSCC_Net: multi-classification deep learning models for diagnosing of skin cancer using dermoscopic images. Cancers, 15(7), p.2179

[7] Naeem, A., Anees, T., Khalil, M., Zahra, K., Naqvi, R.A. and Lee, S.W., 2024. SNC_Net: Skin Cancer Detection by Integrating Handcrafted and Deep Learning-Based Features Using Dermoscopy Images. Mathematics, 12(7), p.1030.

DOI: https://doi.org/10.54216/IJNS.250113
Received: April 25, 2024 Revised: June 01, 2024 Accepted: July 01, 2024

[8] Gururaj, H.L., Manju, N., Nagarjun, A., Aradhya, V.N.M. and Flammini, F., 2023. DeepSkin: a deep learning approach for skin cancer classification. IEEE Access.
[9] Bassel, A., Abdulkareem, A.B., Alyasseri, Z.A.A., Sani, N.S. and Mohammed, H.J., 2022. Automatic malignant and benign skin cancer classification using a hybrid deep learning approach. Diagnostics, 12(10), p.2472.
[10] Sivakumar, M.S., Leo, L.M., Gurumekala, T., Sindhu, V. and Priyadharshini, A.S., 2024. Deep learning in skin lesion analysis for malignant melanoma cancer identification. Multimedia Tools and Applications, 83(6), pp.17833-17853.
[11] Albahli, S. and Nazir, T., 2023. A Circular Box-Based Deep Learning Model for the Identification of Signet Ring Cells from Histopathological Images. Bioengineering, 10(10), p.1147.
[12] Rubiu, G., Bologna, M., Cellina, M., Cè, M., Sala, D., Pagani, R., Mattavelli, E., Fazzini, D., Ibba, S., Papa, S. and Alì, M., 2023. Teeth segmentation in panoramic dental X-ray using mask regional convolutional neural network. Applied Sciences, 13(13), p.7947.
[13] Almutairi, A. and Khan, R.U., 2023. Image-Based Classical Features and Machine Learning Analysis of Skin Cancer Instances. Applied Sciences, 13(13), p.7712.
[14] Ibrahim, D.M., Elshennawy, N.M. and Sarhan, A.M., 2021. Deep-chest: Multi-classification deep learning model for diagnosing COVID-19, pneumonia, and lung cancer chest diseases. Computers in biology and medicine, 132, p.104348.
[15] Albelaihi, A. and Ibrahim, D.M., 2024. DeepDiabetic: An Identification System of Diabetic Eye Diseases Using Deep Neural Networks. IEEE Access.
[16] Zhang, L., Zhang, J., Gao, W., Bai, F., Li, N. and Ghadimi, N., 2024. A deep learning outline aimed at prompt skin cancer detection utilizing gated recurrent unit networks and improved orca predation algorithm. Biomedical Signal Processing and Control, 90, p.105858.
[17] Saeed, M., Naseer, A., Masood, H., Rehman, S.U. and Gruhn, V., 2023. The Power of Generative AI to Augment for Enhanced Skin Cancer Classification: A Deep Learning Approach. IEEE Access, 11, pp.130330-130344.
[18] Naeem, A., Anees, T., Fiza, M., Naqvi, R.A. and Lee, S.W., 2022. SCDNet: a deep learning-based framework for the multiclassification of skin cancer using dermoscopy images. Sensors, 22(15), p.5652.
[19] Zareen, S.S., Sun, G., Kundi, M., Qadri, S.F. and Qadri, S., 2024. Enhancing Skin Cancer Diagnosis with Deep Learning: A Hybrid CNN-RNN Approach. Computers, Materials & Continua, 79(1).
[20] Venugopal, V., Raj, N.I., Nath, M.K. and Stephen, N., 2023. A deep neural network using modified EfficientNet for skin cancer detection in dermoscopic images. Decision Analytics Journal, 8, p.100278.
[21] Babu, R.R. and Philip, F.M., 2024. Optimized deep learning for skin lesion segmentation and skin cancer detection. Biomedical Signal Processing and Control, 95, p.106292.
[22] Prasad, V., GSR, E.S. and MP, R., 2023. ADTBO: Aquila driving training-based optimization with deep learning for skin cancer detection. The Imaging Science Journal, pp.1-19.
[23] Nalluri, S. and Sasikala, R., 2024. A deep neural architecture for SOTA pneumonia detection from chest X-rays. International Journal of System Assurance Engineering and Management, 15(1), pp.489-502.
[24] Saleh, I., Borhan, N., Yunus, A. and Rahiman, W., 2024. Comprehensive Technical Review of Recent Bio-Inspired Population-Based Optimization (BPO) Algorithms for Mobile Robot Path Planning. IEEE Access.
[25] Prabu, E, Gopala, M, and Bobin, A. Enhanced Academic Stress-Coping Skills Assessment in College Students: A Comparative Study of Neutrosophic Distance Measure and Proposed Cubic Pythagorean Fuzzy Hypersoft TOPSIS Method. Journal of International Journal of Neutrosophic Science, vol. 23, no. 4, 2024, pp. 63-82.
[26] Obayya, M.; Alhebri, A.; Maashi, M.; S. Salama, A.; Mustafa Hilal, A.; Alsaid, M.I.; Osman, A.E.; Alneil, A.A. Henry Gas Solubility Optimization Algorithm based Feature Extraction in Dermoscopic Images Analysis of Skin Cancer. Cancers 2023, 15, 2146.
[27] Arumugam, R.V., Saravanan, S. Automated multi-class skin cancer classification using white shark optimizer with ensemble learning classifier on dermoscopy images. Multimed Tools Appl (2024).

DOI: https://doi.org/10.54216/IJNS.250113
Received: April 25, 2024 Revised: June 01, 2024 Accepted: July 01, 2024